Research Square

Preprints are preliminary reports that have not undergone peer review.
They should not be considered conclusive, used to inform clinical practice,
or referenced by the media as validated information.

Two-Stage Synthesis and Antibacterial Profiling of Novel Symmetric and Unsymmetrical 1,2-Dialkylpyrazolium Salts

Nazym A. Alzhapparova
Karaganda National Research University named after Academician E.A. Buketov
Svetlana Yu. Panshina
janim_svetatusik@mail.ru

Karaganda National Research University named after Academician E.A. Buketov
Oxana V. Ponomarenko
Sh. Ualikhanov Kokshetau State University
Marat K. Ibrayev
Karaganda National Research University named after Academician E.A. Buketov
Zhanerke T. Amirkhanova
Karaganda Medical University
Saule B. Akhmetova
Karaganda Medical University
Eugene V. Babaev
Lomonosov Moscow State University
Tulegen M. Seilkhanov
Sh. Ualikhanov Kokshetau State University

Research Article

Keywords: quaternary pyrazolium salts, N-alkylation, NMR spectroscopy, antibacterial activity, Bacillus subtilis

Posted Date: November 11th, 2026

DOI: https://doi.org/10.21203/rs.3.rs-11447934/v1

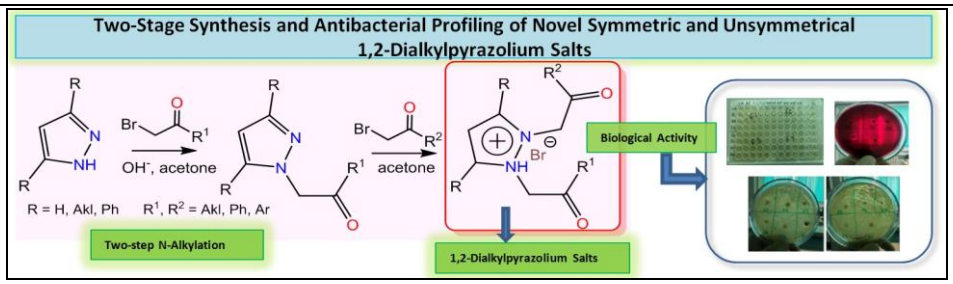
License: This work is licensed under a Creative Commons Attribution 4.0 International License.
Read Full License

Additional Declarations: No competing interests reported.

Two-Stage Synthesis and Antibacterial Profiling of Novel Symmetric and Unsymmetrical 1,2-Dialkylpyrazolium Salts

Nazym A. Alzhapparova [1], Svetlana Yu. Panshina [1]*, Oxana V. Ponomarenko [2], Marat K. Ibrayev [1], Zhanerke T. Amirkhanova [3], Saule B. Akhmetova [3], Eugene V. Babaev [4], Tulegen M. Seilkhanov [2]

[1]*Chemistry Department, Karaganda National Research University named after Academician E.A. Buketov, Karaganda, 100024, Kazakhstan*
e-mail: nazym285@mail.ru, janim_svetatusik@mail.ru, mkibr@mail.ru*
[2]*Chemistry and Biotechnology Department, Sh. Ualikhanov Kokshetau State University, Kokshetau, 020000, Kazakhstan*
e-mail: oksana.ponomarenko.88@mail.ru, tseilkhanov@mail.ru
[3]*Department of Molecular Biology, Biochemistry and Microbiology, Karaganda Medical University, Karaganda, 100012, Kazakhstan*
e-mail: amirhanova@qmu.kz, S.Ahmetova@qmu.kz
[4]*Chemistry Department, Lomonosov Moscow State University, Moscow, 119899, Russia*
e-mail: babaev@org.chem.msu.ru



An efficient two-stage synthetic approach to a novel series of symmetric and unsymmetrical 1,2-dialkylpyrazolium salts was developed via sequential N-alkylation and quaternization of pyrazoles. The quaternization step was found to be critically governed by both electronic and steric effects of substituents at positions 3 and 5 of the pyrazole core. Electron-donating methyl groups facilitate the reaction by enhancing the nucleophilicity of the N-2 pyridine-type nitrogen atom, whereas bulky phenyl rings and strongly electron-withdrawing trifluoromethyl groups arrest quaternization at the mono-alkylation stage. ^{1}H and ^{13}C NMR spectroscopy confirmed the electronic isolation of the pyrazole core from the acyl moiety via the aliphatic -CH_2- linker and demonstrated that C-4 shielding is governed exclusively by the 3,5-substituents. In vitro biological evaluation revealed a narrow antibacterial spectrum with no activity against Candida albicans. The highest susceptibility was observed for Gram-positive *Bacillus subtilis* ATCC 6633. Compound 1,2-bis(2-(4-bromophenyl)-2-oxoethyl)-3,5-dimethyl-1H-pyrazol-1-ium bromide exhibited potent antibacterial activity against *B. subtilis* (inhibition zone 20±1.5 mm), comparable to the reference drug Gentamicin, with a minimum inhibitory concentration (MIC) of 0.12 mg/mL, highlighting it as a promising lead for novel antibacterial agents.

Keywords: quaternary pyrazolium salts, N-alkylation, NMR spectroscopy, antibacterial activity, *Bacillus subtilis*

Introduction

Exhibiting dual acidic and basic properties, the heterocyclic core of pyrazole **1a** combines a nucleophilic pyridine-like nitrogen atom with an acidic pyrrolic N–H center [1–5]. Owing to their versatile, multitarget biological activity, pyrazole-based scaffolds and their reduced or condensed derivatives play a crucial role in drug discovery [6–11]. The mobility of the pyrrolic proton enables prototropic tautomerism [4, 12], while the ambident reactivity of the ring system allows the pyrazole core to readily undergo protonation, *N*-alkylation, *N*-acylation [1–4, 13–17], and quaternization to yield the corresponding pyrazolium salts [13–17].

Quaternary and protic pyrazolium salts are of particular structural, physicochemical, and applied importance [18–32]. Electrostatically, the two adjacent nitrogen atoms induce a unique local positive charge distribution (electrostatic potential profile) that differs significantly from their imidazolium isomers [21]. Effective delocalization of the positive charge across the conjugated π-system endows pyrazolium cations with high chemical and thermal stability [19, 24, 25, 31, 32]. In the solid state and in liquid media, pyrazolium derivatives exhibit rich structural and functional architecture.

Owing to their multiple donor-acceptor centers (N–H … N, N–H … O, N–H … X, where X = Cl, Br), pyrazolium hydrohalides and related salts form extended, highly ordered 2D and 3D hydrogen-bonded networks (e.g., ring graphs $R_2^2(8)$ or orthogonal hydrogen/halogen-bonded motifs) [19–21, 25, 31, 32]. This structural organization makes them useful as organic structure-directing agents

(OSDA/templates) in zeolite synthesis [21] and as active building blocks in supramolecular cocrystals and functional solid-state materials [19–21, 28, 31].

Protic and quaternary pyrazolium salts serve as promising solid proton conductors [18, 27], ionic liquid crystals (ILCs) [27], and ionic liquids (ILs/TPILs) [24–27]. Compared to traditional imidazolium counterparts, pyrazolium-based ILs often display lower viscosity, higher ionic conductivity, wide electrochemical stability windows (>4.0 V), and fine-tunable thermal properties [24–27]. Furthermore, cationic pyrazole derivatives find application as specialized functional dyes (e.g., cationic azo compounds) [29].

In solid-state and solution chemistry, pyrazolium salts serve as key precursors for interconversion into pyrazole coordination complexes and pyrazolates within metal–organic frameworks (MOFs) [28]. Additionally, they exhibit versatile chemical reactivity, undergoing regioselective nucleophilic attacks (e.g., with silyllithium reagents to yield 5-silylated 3-pyrazolines [30]).

On a fundamental photophysical level, time-resolved and photoinduced salt-like (zwitterionic) forms of pyrazole $[Pyrz]^-$ … $[H–Pyrz–H]^+$ provide an efficient non-radiative decay path ($S_1 \rightarrow S_0$) without breaking N–H bonds, explaining the ultrahigh photostability of nitrogen heterocycles [23].

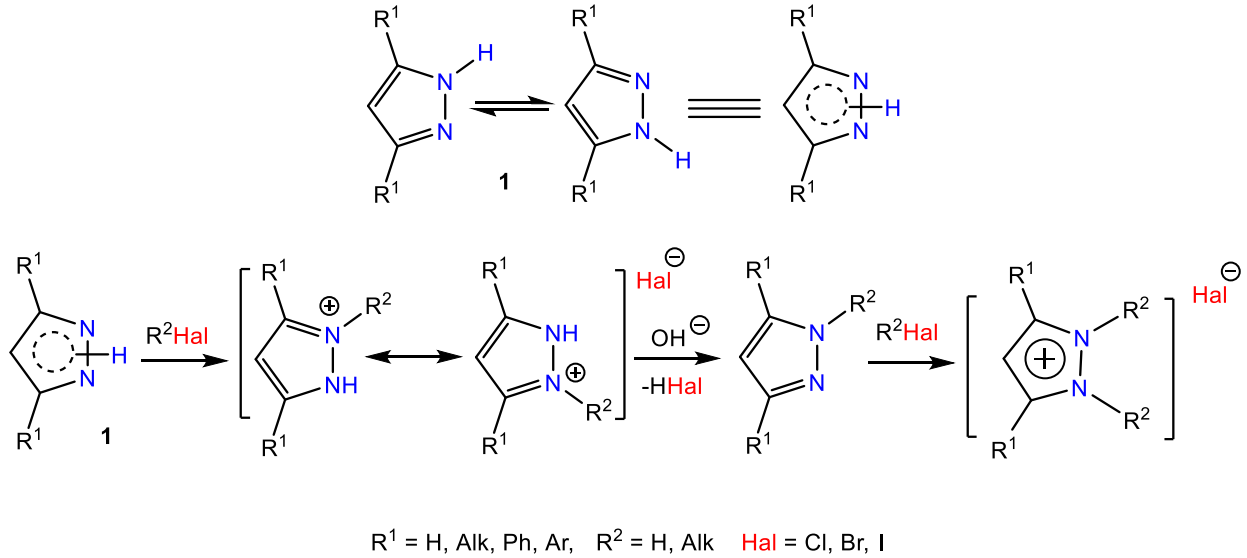
From a biomedical perspective, the relevance of pyrazolium salts is dictated by the critical need to search for novel classes of antibacterial agents to overcome growing antimicrobial resistance [2, 3, 6–11, 22]. Quaternary ammonium compounds and salts of nitrogen heterocycles possessing an amphiphilic structure and a permanent positive charge exhibit high membranotropic activity, enabling them to selectively disrupt pathogen cell membranes [22, 33–35]. Transitioning from monosubstituted N-alkylpyrazoles [36] to symmetrical and unsymmetrical 1,2-disubstituted pyrazolium salts – combining a permanent positive charge with an optimized lipophilic core (via the introduction of t-Bu, Ph, and halogenophenyl radicals) – opens a highly promising route toward potent antimicrobial agents [6–11, 22, 33–35].

Despite significant progress in azole chemistry, methods for the targeted two-step synthesis of 1,2-disubstituted (quaternary) pyrazolium salts using α-bromoketones have remained insufficiently systematized to date [14–16].

Thus, the aim of this study was to develop effective synthetic protocols for the two-step preparation of a novel series of symmetrical and unsymmetrical 1,2-dialkylpyrazolium salts via sequential N-alkylation and quaternization of pyrazoles. Furthermore, we aimed to establish the physicochemical and spectral (^{1}H and ^{13}C NMR) regularities reflecting the impact of substituents on their structure and reactivity, and to systematically evaluate the *in vitro* antibacterial activity of the synthesized compounds against a panel of clinically relevant strains (*Staphylococcus aureus*, *Escherichia coli*, *Bacillus subtilis*, and *Candida albicans*).

Results and Discussion

Direct nucleophilic attack by the unshared electron pair of the moderate-nucleophilicity pyridine-like N-2 nitrogen atom drives the assembly of pyrazolium salts [14–36]. Designing efficient synthetic pathways to these quaternary structures demands a comprehensive accounting of both prototropic tautomeric transformations [1, 4, 12, 36] and the mechanistic specifics of stepwise N-alkylation followed by quaternization [13–17]. Once formed, these azolium salts display exceptional chemical and thermal robustness, primarily imparted by efficient resonance stabilization and positive charge delocalization across the aromatic framework [19, 21, 24, 25, 31, 32]. The prototropic dynamic of initial pyrazole **1** alongside the full synthetic route is illustrated in Scheme 1.



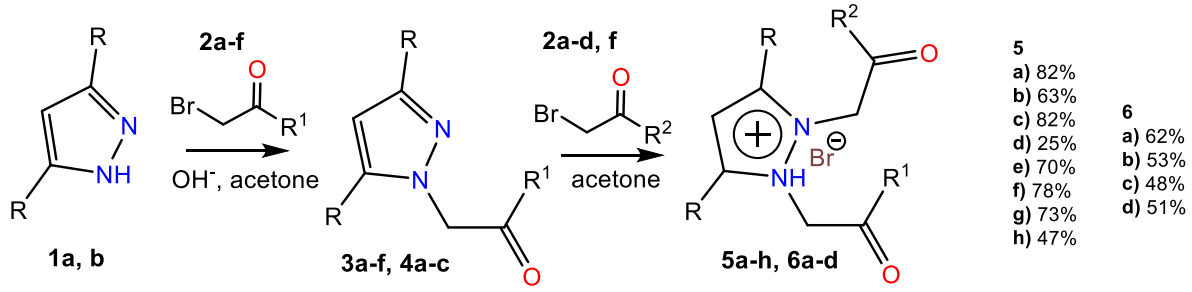
Scheme 1. Tautomerism and Pyrazolium Cation Formation.

The obtained N-monoalkylpyrazoles [36] retain nucleophilic properties and are capable of undergoing quaternization to form pyrazolium salts [14–16]. It is known that the synthesis of such quaternary salts represents

a key step toward obtaining bicyclic systems – pyrazolo[1,2-a]pyrazoles [14–16]. However, only a few examples of the targeted synthesis of 1,2-disubstituted pyrazolium salts via sequential introduction of substituents followed by base-induced cyclization have been reported in the literature [14–16].

Given the high synthetic and biological potential of these heterocycles [6–11], a series of syntheses of new quaternary pyrazolium salts was developed and implemented in the present work. To systematically investigate the reactivity of the pyrazole ring during sequential N-alkylation processes, we evaluated the contribution of both electronic and steric effects of substituents at positions 3 and 5 of the starting heterocycles **1a–d**. The α-bromoketones **2a–f**, containing branched aliphatic or aromatic moieties with electron-donating and electron-withdrawing substituents, were utilized as alkylating agents.

The synthetic route to mono- (**3**, **4**, **7**, **8**) and 1,2-disubstituted pyrazolium salts (**5**, **6**) is depicted in Schemes 2 and 3.



1
a) R = H
b) R = CH_3

2
a) $R^1 = R^2$ = t-Bu
b) $R^1 = R^2$ = Ph
c) $R^1 = R^2$ = 4-Br-C_6H_4
d) $R^1 = R^2$ = 4-F-C_6H_4
e) $R^1 = R^2$ = 4-CF_3O-C_6H_4
f) $R^1 = R^2$ = 4-NO_2-C_6H_4

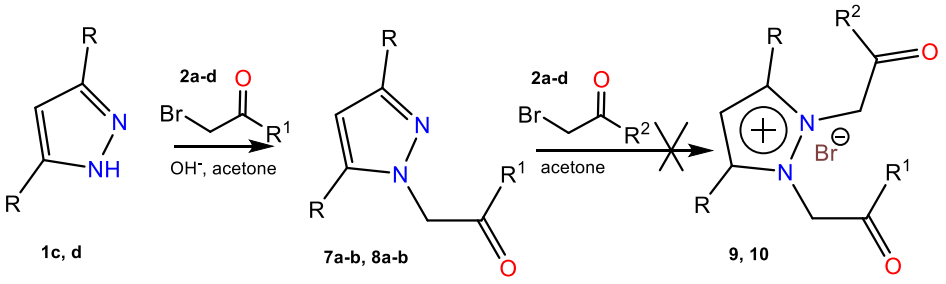
3
a) R = H, R^1 = t-Bu
b) R = H, R^1 = Ph
c) R = H, R^1 = 4-Br-C_6H_4
d) R = H, R^1 = 4-F-C_6H_4
e) R = H, R^1 = 4-CF_3O-C_6H_4
f) R = H, R^1 = 4-NO_2-C_6H_4

4
a) R = CH_3, R^1 = t-Bu
b) R = CH_3, R^1 = Ph
c) R = CH_3, R^1 = 4-Br-C_6H_4

5
a) R = H, $R^1 = R^2$ = t-Bu
b) R = H, $R^1 = R^2$ = Ph
c) R = H, $R^1 = R^2$ = 4-F-C_6H_4
d) R = H, $R^1 = R^2$ = 4-NO_2-C_6H_4
e) R = H, R^1 = 4-CF_3O-C_6H_4, R^2 = t-Bu
f) R = H, R^1 = 4-F-C_6H_4, R^2 = t-Bu
g) R = H, R^1 = 4-F-C_6H_4, R^2 = Ph
h) R = H, R^1 = 4-Br-C_6H_4, R^2 = Ph

6
a) R = CH_3, $R^1 = R^2$ = t-Bu
b) R = CH_3, $R^1 = R^2$ = Ph
c) R = CH_3, $R^1 = R^2$ = 4-Br-C_6H_4
d) R = CH_3, R^1 = 4-Br-C_6H_4, R^2 = Ph

Scheme 2. Two-step synthesis of 1,2-disubstituted pyrazolium bromides **5a–h**, **6a–d** based on sequential N-alkylation of pyrazoles **1a, b**.



1
c) R = Ph
d) R = CF_3

2
a) $R^1 = R^2$ = t-Bu
b) $R^1 = R^2$ = Ph
c) $R^1 = R^2$ = 4-Br-C_6H_4
d) $R^1 = R^2$ = 4-F-C_6H_4

7, 9
a) R = Ph, $R^1 = R^2$ = t-Bu
b) R = Ph, $R^1 = R^2$ = Ph
c) R = Ph, $R^1 = R^2$ = 4-Br-C_6H_4

8, 10
a) R = CF_3, $R^1 = R^2$ = t-Bu
b) R = CF_3, $R^1 = R^2$ = Ph
c) R = CF_3, $R^1 = R^2$ = 4-F-C_6H_4

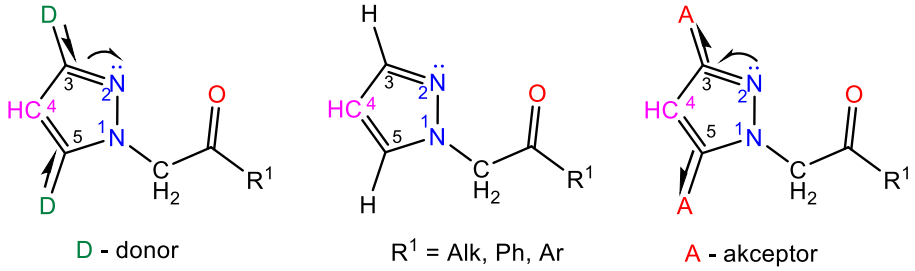
Scheme 3. Mono-N-alkylation of 3,5-diphenyl- (**1c**) and 3,5-bis(trifluoromethyl)- (**1d**) pyrazoles and deactivation of the reaction center at the quaternization stage.

It was established that the nature of the substituent R at positions 3 and 5 in the starting pyrazole critically influences the success of the second stage – quaternization of the monoalkylated intermediates to the target pyrazolium salts. The synthesis of the target compounds involves two sequential stages. The first stage (mono-N-alkylation) is carried out in the presence of a base [36], which facilitates the smooth formation of neutral mono-derivatives **3a–f** and **4a–c**. The second stage (quaternization) proceeds in a neutral medium under the action of the corresponding α-bromoketone. The introduction of the first phenacyl or pinacolyl group somewhat reduces the nucleophilicity of the remaining "pyridine" nitrogen atom.

Nevertheless, the salt formation reaction is successfully completed due to the moderate donor properties of the methyl groups (in the case of dimethyl derivative **1b**) or the absence of steric hindrance (in the case of unsubstituted pyrazole **1a**). At the same time, the substituents significantly affect the reaction rate: while for substrate **1b** (R = CH_3) the second stage is completed within 24 hours, pyrazole **1a** (R = H) requires more time for the second stage – up to 3 days. As a result, a wide series of both symmetrical (R^1 = R^2 compounds **5a–d**, **6a–c**) and structurally unique unsymmetrical ($R^1 \neq R^2$, compounds **5e–h**, **6d**) pyrazolium salts was obtained.

Upon moving to 3,5-diphenyl- (**1c**) and 3,5-bis(trifluoromethyl)pyrazoles (**1d**), the picture changes drastically (Scheme 3). It was found that the reaction strictly halts at the stage of formation of monoalkylated products **7a–b** and **8a–b**. Attempts to carry out their further quaternization under analogous conditions failed to yield salts **9** and **10**.

The reasons for such behavior can be attributed to the following two key factors: first, the presence of phenyl rings (R = Ph) at positions 3 and 5 creates significant steric hindrance around the N-reaction center, physically preventing the bulky incoming α-bromoketone from approaching the nitrogen atom to undergo nucleophilic substitution; second, the trifluoromethyl group (R = CF_3) acts as a powerful electron-withdrawing group via its –I effect, where two CF_3-groups deactivate the conjugated pyrazole ring system and reduce the electron density on the "pyridine" nitrogen atom so strongly (Scheme 4) that its nucleophilicity becomes insufficient for quaternization to proceed, even with active substrates.



Scheme 4. Influence of the electronic effects of substituents at positions 3 and 5 of the pyrazole ring on the nucleophilicity of the "pyridine" nitrogen atom.

To evaluate the reactivity and electronic structure of the synthesized N-phenacyl- and N-pinacolylpyrazoles **3a,b**, **4a,b**, **7a,b**, and **8a,b**, a detailed analysis of their ^{1}H (Table 1) and ^{13}C NMR spectra (Table 2) was performed. The key factor determining the physicochemical properties of these systems is the electronic effect of substituents at positions 3 and 5 of the pyrazole ring on electron density distribution. As shown in Scheme 4, donor substituents increase the electron density on the lone pair of the nitrogen atom (N-2), whereas acceptor substituents decrease it.

The variation in electron density also affects the unsubstituted carbon and hydrogen atoms of the CH-fragment at position 4 of the pyrazole ring. This fundamental regularity can be indirectly traced via the chemical shifts of the adjacent protons in ^{1}H NMR spectra of N-pinacolylpyrazoles **3a**, **4a**, **7a**, **8a** and N-phenacylpyrazoles **3b**, **4b**, **7b**, **8b** (Table 1).

Table 1. Chemical shifts in ^{1}H NMR spectra (δ, ppm, *J* in Hz) of compounds **3a,b**, **4a,b**, **7a,b**, and **8a,b**

Compound	Functional groups and corresponding ^{1}H NMR chemical shifts δ (ppm, *J*/Hz)				
	R	R-3, R-5 (Pyr)	**CH-4 (Pyr)**	CH_2	COR^1 R^1 = t-Bu (**a**), Ph (**b**)
3a[15, 36] ($CDCl_3$)	R = H	8.54 (1H, d, *J* = 3.0) 8.08 (1H, d, *J* = 6.8)	**6.71** **(1H, t, *J* = 3.0)**	4.67 (2H, s)	1.28 (9H, s, $C(CH_3)_3$)
3b[15, 36] ($CDCl_3$)	R = H	7.54 (1H, d, *J* = 2.6) 7.44 (1H, d, *J* = 2.6).	**6.31** **(1H, t, *J* = 4.4)**	5.54 (2H, s)	7.95 – 7.89 (2H, m, Ph) 7.59 – 7.52 (1H, m, Ph) 7.48 – 7.42 (2H, m, Ph)
4a[36] (DMSO-d_6)	R = CH_3	2.05 (3H, s, CH_3) 2.00 (3H, s, CH_3)	**5.82** **(1H, s)**	5.15 (2H, s)	1.14 (9H, s, $C(CH_3)_3$)
4b[36] (DMSO-d_6)	R = CH_3	2.06 (3H, s, CH_3) 2.05 (3H, s, CH_3)	**5.83** **(1H, s)**	5.64 (2H, s)	8.01 (2H, d, *J* = 7.9, Ph) 7.67 (1H, t, *J* = 7.5, Ph) 7.55 (2H, t, *J* = 7.7, Ph)
7a[36] (DMSO-d_6)	R = Ph	7.81 (2H, d, *J* = 7.1, Ph) 7.46 – 7.42 (2H, m, Ph) 7.42 – 7.35 (5H, m, Ph) 7.29 (1H, t, *J* = 7.3, Ph)	**6.87** **(1H, s)**	5.34 (2H, s)	1.02 (9H, s, $C(CH_3)_3$)
7b[36] (DMSO-d_6)	R = Ph	7.82 (2H, d, *J* = 7.0) 7.48 – 7.35 (8H, m, Ph)	**6.95** **(1H, s)**	5.88 (2H, s)	7.98 (2H, d, *J* = 7.2, Ph) 7.66 (1H, t, *J* = 7.4, Ph) 7.52 (2H, t, *J* = 7.7, Ph)

8a ($CDCl_3$)	R = CF_3	–	**6.92 (1H, s)**	5.31 (2H, s)	1.23 (9H, s, $C(CH_3)_3$)
8b ($CDCl_3$)	R = CF_3	–	**6.96 (1H, s)**	5.77 (2H, s)	7.91 (2H, d, *J* = 7.5, Ph) 7.62 (2H, d, *J* = 7.3, Ph) 7.48 (1H, t, *J* = 7.6, Ph)

Analysis of the chemical shifts of the pyrazole ring CH-4 proton (Table 1) indicates a pronounced sensitivity of this position to the electronic effects of substituents at the symmetrical 3 and 5 positions. In the spectra of compounds **3a,b** (R = H)**,** which are unsubstituted at the ring carbon atoms, the CH-4 proton signal appears for **3a** (R^1 = t-Bu) as a triplet at δ 6.71 ppm and for **3b** (R^1 = Ph) at δ 6.31 ppm. The introduction of methyl groups in compounds **4a,b**, which exhibit positive inductive (+I) and hyperconjugation effects, leads to a significant increase in electron density at CH-4. As a result, strong shielding of the CH-4 proton is observed, with its signal shifting upfield to δ 5.82–5.83 ppm (the upfield shift for **4a,b** relative to **3a,b** is approximately 0.5–0.9 ppm).

Replacement of the hydrogen atoms with phenyl substituents in **7a,b** is accompanied by deshielding of the CH-4 proton center (≈ δ 6.87–6.95 ppm). Despite the formally possible weak electron-donating conjugation effect, the aromatic rings shift the signal downfield relative to the unsubstituted analogs due to their spatial orientation, –I effect, and ring current deshielding effects.

The most pronounced deshielding effect is observed upon the introduction of strongly electron-withdrawing trifluoromethyl (CF_3) groups (compounds **8a,b**). Possessing a powerful –I effect, the CF_3-groups effectively pull electron density away from the pyrazole core; consequently, the CH-4 proton signal predictably shifts to the most downfield region of the spectrum and is recorded at δ 6.92 ppm (**8a**) and 6.96 ppm (**8b**).

The trends observed in the ^{1}H NMR spectra are in full agreement with the changes in the chemical shifts of the pyrazole ring ^{13}C nuclei at the C-4 position, which is traditionally the most nucleophilic center in pyrazoles (Table 2).

Table 2. Chemical shifts in ^{13}C NMR spectra (δ, ppm, *J* in Hz) of compounds **3a,b**, **4a,b**, **7a,b**, and **8a,b**

Compound	Functional groups and corresponding ^{13}C NMR chemical shifts δ (ppm, *J*/Hz)					
	R	R-3, R-5 (Pyr)	**CH-4 (Pyr)**	CH_2	C=O	R^1 R^1 = t-Bu (**a**), Ph (**b**)
3a[15, 36] ($CDCl_3$)	R = H	139.3 (CH) 129.8 (CH)	**107.5 (CH)**	56.5	205.9	43.9 ($\underline{C}(CH_3)_3$) 26.3 ($C(\underline{CH_3})_3$)
3b[15, 36] ($CDCl_3$)	R = H	139.9 (CH) 134.1 (CH)	**106.6 (CH)**	57.8	192.6	134.7 (C, Ph), 131.0 (CH, Ph), 129.0 (CH, Ph), 128.2 (CH, Ph)
4a[36] (DMSO-d_6)	R = CH_3	146.3 (C), 13.6 (CH_3) 140.7 (C), 10.9 (CH_3)	**105.4 (CH)**	53.9	209.6	43.7 ($\underline{C}(CH_3)_3$) 26.3 ($C(\underline{CH_3})_3$)
4b[36] (DMSO-d_6)	R = CH_3	146.7 (C), 13.8 (CH_3) 140.6 (C), 11.0 (CH_3)	**105.4 (CH)**	55.7	194.5	135.1, 134.5, 129.5, 128.7 (Ph)
7a[36] (DMSO-d_6)	R = Ph	150.2 (C), 145.9 (C) 133.6, 130.6, 129.3, 129.3, 129.2, 128.9, 128.2, 125.6 (Ph)	**104.0 (CH)**	55.5	209.5	43.4 ($\underline{C}(CH_3)_3$) 26.2 ($C(\underline{CH_3})_3$)
7b[36] (DMSO-d_6)	R = Ph	150.5 (C), 146.3 (C), 134.8, 134.7, 133.6, 130.5, 129.5, 129.5, 129.3, 129.2, 128.7, 128.2, 125.7, 125.6 (Ph)	**100.2 (CH)**	57.1	194.4	134.8, 134.7, 133.6, 130.5, 129.5, 129.5, 129.3, 129.2, 128.7, 128.2, 125.7, 125.6 (Ph)
8a ($CDCl_3$)	R = CF_3	142.5 (q, *J* = 39.4, C) 134.2 (q, *J* = 40.3, C) 119.8 (qd, *J* = 269.2, 125.3, $2CF_3$)	**106.6 (CH)**	56.5	205.4	43.5 ($\underline{C}(CH_3)_3$) 26.2 ($C(\underline{CH_3})_3$)
8b ($CDCl_3$)	R = CF_3	142.6 (q, *J* = 39.3, C), 134.7 (q, *J* = 40.4, C), 119.8 (qd, *J* = 269.1, 128.1, $2CF_3$)	**106.7 (CH)**	57.9	189.9	134.7 (CH, Ph) 133.7 (C, Ph) 129.2 (2CH, Ph) 128.1 (2CH, Ph)

For compounds with methyl groups (**4a,b**), the CH-4 carbon signal is located in the region of δ 105.4 ppm, emphasizing the high electron density at this atom under the influence of electron-donating substituents.

In the case of phenyl derivatives (**7a,b**), the highest shielding of the CH-4 carbon nucleus is observed (≈ δ 100.2–104.0 ppm), which may be attributed to the efficient redistribution of π-electron density within the conjugated system of the heteroaryl core in the ground state, despite the local deshielding of the attached proton.

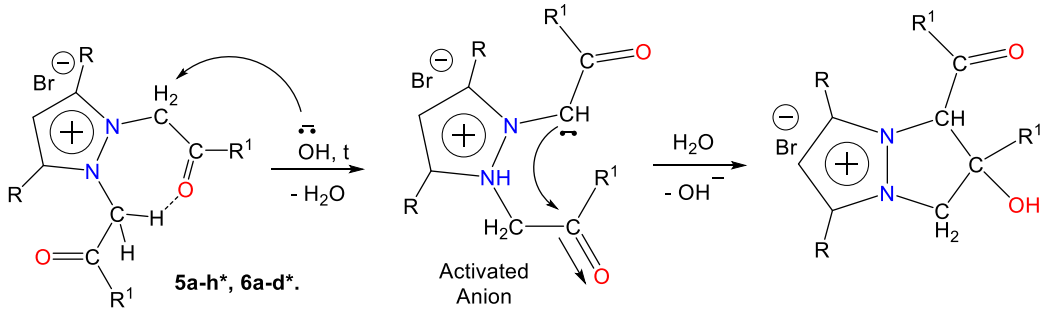
For the trifluoromethyl derivatives (**8a,b**), the CH-4 signal shifts downfield to 106.6–106.7 ppm relative to the systems with phenyl moieties **7a,b**, confirming the overall electron deficiency of the ring caused by the strong electron-withdrawing effect of the two CF_3-groups. It is interesting to note that varying the R^1 substituent (R^1 = t-Bu

(**a**), Ph (**b**)) in the acyl fragment exerts virtually no influence on the electron density of the pyrazole core itself. This indicates spatial and electronic isolation of the pyrazole ring from the acyl radical due to the intervening aliphatic -CH_2- linker, which effectively blocks the transmission of inductive and mesomeric effects. The effect of the R^1 group is localized on the carbonyl carbon (C=O), where replacing the *tert*-butyl group (**3a**, **4a**, **7a**, **8a**) with a phenyl group (**3b**, **4b**, **7b**, **8b**) induces a strong upfield shift (by an average of $\Delta\delta$ = 13–15 ppm) due to conjugation of the carbonyl with the benzene ring.

Thus, the electron density of the pyrazole ring in the investigated series of compounds **3a**,**b 4a,b, 7a,b**, and **8a,b** is governed exclusively by the nature of the substituents at positions 3 and 5. The introduction of electron-donating substituents (compounds **4a–c**) represents a direct route to increasing the yields of quaternary pyrazolium salts under mild conditions. Conversely, the introduction of electron-withdrawing substituents blocks or significantly hinders this process, requiring stringent activation of the electrophilic reagent in the case of compounds **7a–c** and **8a–c**.

The salts **5a–h** and **6a–d** obtained in our work are high-melting, finely dispersed white powders that are insoluble in nonpolar organic solvents and poorly soluble in polar media even upon boiling.

Based on literature data from X-ray diffraction analysis of N-pyrazolium hydrochloride and hydrobromide derivatives [31, 32], it can be assumed that their low solubility is attributed to the formation of a strong system of inter- and intramolecular hydrogen bonds within the crystal lattice, leading to the formation of associates **5a–h*** and **6a–d*** (Scheme 5).



Scheme 5. Intramolecular cyclization of salts **5a–h*** and **6a–d*** under alkaline conditions

However, these associates **5a–h*** and **6a–d*** are disrupted upon heating in an alkaline medium. Under these conditions, deprotonation activates an intramolecular aldol addition: the generated carbanion attacks the spatially adjacent carbonyl group (the interaction of which in the starting salt was supported by an intramolecular hydrogen bond), leading to ring closure and the formation of the heterocyclic system [14–16]. The proposed mechanism of intramolecular aldol addition qualitatively explains the experimentally observed necessity for harsh conditions (heating, alkaline medium) to break the strong system of intermolecular bonds in the starting salts **5a–h*** and **6a–d***.

Thus, a systematic study of the reactivity of pyrazoles **1a–d** in two-fold N-alkylation reactions made it possible to establish the key patterns of salt formation processes. Thus, the success of the quaternization of monoalkylated intermediates to the target 1,2-disubstituted pyrazolium salts (**5a–h**, **6a–d**) is directly determined by the nature of the substituents at positions 3 and 5 of the pyrazole ring. Electron-donating methyl groups (**1b**) accelerate the reaction by increasing the nucleophilicity of the N-2 atom, whereas sterically bulky phenyl (**1c**) and strongly electron-withdrawing trifluoromethyl groups (**1d**) strictly block quaternization at the stage of mono-derivative formation (**7a–c**, **8a–c**).

Spectral analysis (^{1}H and ^{13}C NMR) confirmed the isolation of the pyrazole core from the R^1 acyl radical via the –CH_2– linker and clearly demonstrated the shielding/deshielding trends of the C-4 carbon center depending on the electronic effects of the R-groups.

Biological Activity

Pyrazoles represent an exceptionally versatile class of nitrogen-containing heterocycles that occupy a central role in modern medicinal chemistry due to their broad spectrum of biological activities [1, 6–11, 36]. The unique acid–base profile and structural flexibility of the pyrazole core allow for precise tuning of its lipophilicity, hydrogen-bonding capacity, and electronic features, making it a privileged scaffold for drug design [6–11]. Pyrazole-based molecules exhibit remarkable efficacy against various Gram-positive and Gram-negative bacterial strains, as well as fungal pathogens [38–42]. Their mechanism often involves membrane-disrupting (membranotropic) effects driven by amphiphilic cations [22, 33–35]. Substituted pyrazole derivatives, particularly those bearing oxime or hydrazone functional moieties, demonstrate pronounced activity against diverse viral targets [43]. The pyrazole ring serves as the key pharmacophore in non-steroidal anti-inflammatory drugs (NSAIDs) and selective COX-2 inhibitors (e.g., deracoxib, celecoxib) [44].

In our previous work, cytotoxicity screening [36] of monosubstituted N-alkylpyrazoles (**3a–c,f**, **4b**, **7b**, etc.) provided valuable insights into the structure–property relationships (SPR) governing their membranotropic properties. It was demonstrated that modulating the electronic effects of ring and N-phenacyl substituents – by introducing electron-donating methyl or electron-withdrawing phenyl groups – significantly impacts biological activity. Building upon these regularities,

transitioning to 1,2-disubstituted pyrazolium salts offers a promising strategy to optimize charge distribution and lipophilicity, ultimately paving the way toward novel, highly potent antimicrobial agents capable of addressing antimicrobial resistance [6–11, 22, 33–35].

It is well known [22, 33–35] that quaternary ammonium compounds and nitrogen heterocycle salts possess a pronounced affinity for the cell walls of microorganisms and exhibit high antimicrobial activity. In this context, the transition from mono-derivatives to symmetrical pyrazolium salts (**5a–c, e–h**, **6b–d**), combining two functionalized intermediates within a single structure, represented a logical extension of this work. The presence of a permanent positive charge on the heterocycle, together with optimized lipophilicity (achieved via the introduction of *t*-Bu-, Ph-, or halogenated phenyl radicals), should contribute to increasing their selectivity. At the next stage, we systematically studied the antibacterial properties of the synthesized symmetrical pyrazolium salts against a panel of strains of Gram-positive (*Staphylococcus aureus* ATCC 6538, *Bacillus subtilis* ATCC 6633) and Gram-negative (*Escherichia coli* ATCC 25922) bacteria, as well as yeast-like fungi (*Candida albicans* ATCC 10231). The results of the antimicrobial activity evaluation are presented in Table 3.

Table 3. Antimicrobial activity of compounds **5a–c**, **e–h**, and **6b–d** against the test strains studied

Compound		Test strain			
		S. aureus (ATCC 6538)	*E. coli (ATTC 25922)*	*B. subtilis (ATTC 6633)*	*C. albicans (ATTC 10231)*
		Zone of inhibition diameter, mm ($M \pm m$)			
5a	R = H, $R^1 = R^2$ = t-Bu	0±0.00	0±0.00	0±0.00	0±0.00
5b	R = H, $R^1 = R^2$ = Ph	0±0.00	0±0.00	0±0.00	0±0.00
5c	R = H, $R^1 = R^2$ = 4-F-C_6H_4	10±0.00	10±0.00	0±0.00	0±0.00
5e	R = H, R^1 = 4-CF_3O-C_6H_4, R^2 = t-Bu	0±0.00	11±1.7	10±0.00	0±0.00
5f	R = H, R^1 = 4-F-C_6H_4, R^2 = t-Bu	10±2.31	0±0.00	0±0.00	0±0.00
5g	R = H, R^1 = 4-F-C_6H_4, R^2 = Ph	0±0.00	10±1.15	14±0.58	0±0.00
5h	R = H, R^1 = 4-Br-C_6H_4, R^2 = Ph	0±0.00	11±1.2	10±1.15	0±0.00
6b	R = CH_3, $R^1 = R^2$ = Ph	0±0.00	0±0.00	0±0.00	0±0.00
6c	R = CH_3, $R^1 = R^2$ = 4-Br-C_6H_4	11±0.6	10±0.58	20±1.5	0±0.00
6d	R = CH_3, R^1 = 4-Br-C_6H_4, R^2 = Ph	10±1.73	10±2.89	16±1.73	0±0.00
Gentamicin (control)		20±0.58	19±1.73	20±0.58	–
Nystatin (control)		–	–	–	18±0.58

It was established that the studied samples exhibit varying degrees of antimicrobial activity. Against the Gram-positive strain *Staphylococcus aureus* (ATCC 6538), the highest activity was displayed by compounds **6c** (11±0.6 mm), **6d** (10±1.73 mm), **5c** (10±0.00 mm), and **5f** (10± 2.31 mm). Compared to the reference drug (gentamicin, 20±0.58 mm), the effect of these compounds can be characterized as moderate. The remaining samples showed no antibacterial activity against *S. aureus* (0±0.00 mm).

Against the Gram-negative culture *Escherichia coli* (ATCC 25922), activity was detected for compounds **5c**, **5e**, **5g**, **5h**, **6c**, and **6d**. The inhibition zone diameters ranged from 10 to 11 mm (for compounds **5e** and **5h**: 11±1.7 mm and 11±1.2 mm, respectively; for **5c**, **5g**, **6c**, and **6d**: 10 mm with corresponding margins of error), indicating a weak inhibitory effect compared to the control (19±1.73 mm).

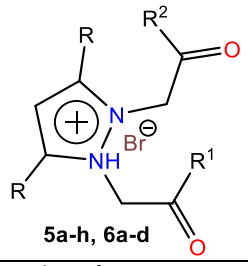
The highest sensitivity to the tested substances was noted for the *Bacillus subtilis* (ATCC 6633) strain. Compound **6c** exhibited high antibacterial activity (20 ±1.5 mm), comparable to the reference drug (20±0.58 mm). Compounds **6d** and **5g** demonstrated moderate activity (16±1.73 mm and 14±0.58 mm, respectively), whereas weak activity was recorded for samples **5e** and **5h** (10±0.00 mm and 10±1.15 mm).

None of the tested compounds showed antifungal activity against *Candida albicans* (ATCC 10231) (no zones of inhibition were detected).

The minimum inhibitory concentration (MIC) determination results are presented in Table 4. The MIC values varied depending on the microorganism species, indicating the selectivity of action of the studied compounds.

Table 4. Minimum inhibitory concentration (MIC) of compounds **5a–c**, **e–h**, and **6b–d** against the test strains studied

Compound	Test strain



5a-h, 6a-d

		S. aureus (ATCC 6538)	*E. coli (ATTC 25922)*	*B. subtilis (ATTC 6633)*	*C. albicans (ATTC 10231)*
		MIC, mg/mL			
5a	R = H, R^1 = R^2 = t-Bu	growth	growth	growth	growth
5b	R = H, R^1 = R^2 = Ph	growth	growth	growth	growth
5c	R = H, R^1 = R^2 = 4-F-C_6H_4	0.5	0.5	growth	growth
5e	R = H, R^1 = 4-CF_3O-C_6H_4, R^2 = t-Bu	growth	0.5	1.0	growth
5f	R = H, R^1 = 4-F-C_6H_4, R^2 = t-Bu	0.5	growth	growth	growth
5g	R = H, R^1 = 4-F-C_6H_4, R^2 = Ph	growth	0.5	0.5	growth
5h	R = H, R^1 = 4-Br-C_6H_4, R^2 = Ph	growth	0.5	0.5	growth
6b	R = CH_3, R^1 = R^2 = Ph	growth	growth	growth	growth
6c	R = CH_3, R^1 = R^2 = 4-Br-C_6H_4	0.5	0.5	0.12	growth
6d	R = CH_3, R^1 = 4-Br-C_6H_4, R^2 = Ph	0.5	0.5	0.25	growth

Thus, against *S. aureus* (ATCC 6538), the MIC values for the active compounds (**5c**, **5f**, **6c**, and **6d**) were 0.5 mg/mL. For the Gram-negative strain *E. coli* (ATCC 25922), similar values (MIC = 0.5 mg/mL) were observed for samples **5c**, **5e**, **5g**, **5h**, **6c**, and **6d**.

The studied compounds exhibited the highest activity against *B. subtilis* (ATCC 6633). Compound **6c** was characterized by the lowest MIC value (0.12 mg/mL), for sample **6d** this indicator was 0.25 mg/mL, and for compounds **5g** and **5h** it was 0.5 mg/mL. The lowest activity in this series was shown by sample **5e** with an MIC of 1.0 mg/mL.

Against the fungal culture *C. albicans* (ATCC 10231), MIC determination was impossible due to confluence growth of the test strain for all tested samples.

Thus, the conducted systematic study of the antimicrobial properties and minimum inhibitory concentration (MIC) values of the new symmetrical pyrazolium salts (**5a–c**, **e–h**, and **6b–d**) enabled the identification of key structure–activity relationships. Specifically, the studied compounds exhibited a narrow spectrum of action, displaying activity exclusively against bacterial strains while remaining inactive against the test culture *Candida albicans* (ATCC 10231).

The Gram-positive spore-forming strain *Bacillus subtilis* (ATCC 6633) exhibited the highest susceptibility to the tested salts, whereas the compounds demonstrated moderate to weak inhibitory activity against *Staphylococcus aureus* (ATCC 6538) and the Gram-negative culture *Escherichia coli* (ATCC 25922).

Based on the obtained data regarding inhibition zone diameters and minimum inhibitory concentrations, compound **6c** was identified as the most promising. It exhibited high antibacterial activity against *B. subtilis*, comparable to the reference drug gentamicin (20±1.5 mm vs. 20±0.58 mm, respectively), and showed the lowest MIC value among all tested samples (0.12 mg/mL).

Compounds **6c** and **6d** compare favorably due to their higher potency and broader spectrum of antibacterial response, confirming the viability of the chosen strategy – optimizing lipophilicity and modifying substituents in the pyrazole core – for designing novel, effective antibacterial agents.

Experimental

Materials and methods. Starting materials **1a–d** and **2a–f** (Acros, Merck) were used as received. Reaction progress and product purity were monitored by TLC on Silufol plates (visualization with I_2 vapor). Melting and boiling points were measured in open capillaries using a Büchi M560 apparatus. NMR spectra (^{1}H – 400 MHz, ^{13}C – 100 MHz, ^{19}F – 376 MHz) and 2D correlation experiments were recorded on a Bruker AVANCE III HD spectrometer in DMSO-d_6 (δ_H 2.50, δ_C 40.03) and D_2O (δ_H 4.70). Tetramethylsilane (^{1}H, ^{13}C) and $CFCl_3$ (^{19}F) were used as internal standards. Coupling constants are given in Hz. GC-MS analysis was performed on an Agilent 7890A GC / 5975C MSD system equipped with an Rtx DHA-100 column (carrier gas: He; samples in acetone; run time: 32 min). IR spectra were recorded on an FSM 1201 FT-IR instrument in KBr pellets (400 – 4000 cm^{-1}).

Antimicrobial and antifungal activities were determined using the disk diffusion method [45–49], and the minimum inhibitory concentration (MIC) was determined by the serial microdilution method in liquid nutrient medium [50, 51]. All assays were performed in triplicate (n = 3). The following test strains were used to evaluate antimicrobial activity: *Staphylococcus aureus* (ATCC 6538), *Escherichia coli* (ATCC 25922), *Bacillus subtilis* (ATCC 6633), and *Candida albicans* (ATCC 10231). Commercial culture media from HiMedia were used for the assays: meat-peptone agar, mannitol salt agar (egg yolk emulsion), Endo agar, and Sabouraud dextrose agar. Data were statistically processed and are presented as mean values (M) and standard error of the mean (m).

Synthetic Procedures

General Synthetic Procedure for *N*-alkylpyrazoles (3a–f, 4a–c, 7a–c, 8a–c). The synthetic procedures and spectral characterization data for compounds **3a–c**, **3e–i**, **4a–c**, and **7a–c** were reported previously [36].

Synthesis of 1-(4-fluorophenyl)-2-(1H-pyrazol-1-yl)ethan-1-one (3d). To a solution of pyrazole **1a** (2.0 g, 29.4 mmol) in anhydrous acetone (50 mL), anhydrous

potassium carbonate (4.0 g, 29.4 mmol) was added under stirring. Subsequently, 2-bromo-1-(4-fluorophenyl)ethan-1-one **2d** (6.4 g, 29.4 mmol) was added to the reaction mixture. The resulting mixture was stirred at room temperature for 24 h. Upon completion of the reaction, the inorganic salts were filtered off, and the filtrate was concentrated under reduced pressure using a rotary evaporator. The crude solid product N-(4-fluorophenacyl)pyrazole **3d** was collected and dried in air.

Yield of **3d** 4.5 g (75%), light beige crystals, mp 124 °C. IR spectrum, ν, cm^{-1}: 3113 (CH), 2990, 2947 (CH_2), 1701 (C=O), 1620 (C=N), 1230 (C–F), 1149 (C–F) (Fig. S1). ^1H NMR spectrum ($CDCl_3$), δ, ppm (*J*, Hz): 8.01–7.92 (2H, m, Ar); 7.55 (1H, d, *J* = 2.0, Pz); 7.46 (1H, d, *J* = 2.3, Pz); 7.18–7.09 (2H, m, Ar); 6.33 (1H, t, *J* = 2.3, Pz); 5.54 (2H, s, CH_2) (Fig. S2). ^{13}C NMR spectrum ($CDCl_3$), δ, ppm: 191.14 (C=O); 167.59 (C–F, Ar); 165.04 (C–F, Ar); 140.14 (CH, Pz); 131.05 (CH, Ar); 131.00 (CH, Pz); 130.96 (CH, Ar); 116.19 (CH, Ar); 106.74 (CH, Pz); 57.67 (CH_2) (Fig. S3). GC-MS Retention time 14.225 min, m/z (EI): 204, 203, 176, 123, 95, 81, 77, 54, 28 (Fig. S4).

The synthesis of 1-(*tert*-butyl)-2-(3,5-bis(trifluoromethyl)-1H-pyrazol-1-yl)ethan-1-one (8a), 1-phenyl-2-(3,5-bis(trifluoromethyl)-1H-pyrazol-1-yl)ethan-1-one (8b) and 1-(4-fluorophenyl)-2-(3,5-bis(trifluoromethyl)-1H-pyrazol-1-yl)ethan-1-one (8c) was carried out according to procedure for the preparation of (**3d**), using appropriate reagents.

Yield of **8a** 5.6 g (63%), light pink crystals, mp 32 °C. IR spectrum, ν, cm^{-1}: 3155 (CH), 2986, 2955 (CH_3), 1728 (C=O), 1589 (C=N), 1138 (C–F) (Fig. S5). ^1H NMR spectrum ($CDCl_3$), δ, ppm (*J*, Hz): 6.92 (1H, s, Pz); 5.31 (2H, s, CH_2); 1.23 (9H, s, $C(CH_3)_3$) (Fig. S6). ^{13}C NMR spectrum ($CDCl_3$), δ, ppm (*J*, Hz): 205.35 (C=O); 142.45 (q, *J* = 39.4, C–CF_3, Pz); 134.24 (q, *J* = 40.3, C–CF_3, Pz); 119.75 (qd, *J* = 269.2, *J* = 125.3, 2CF_3); 106.62 (CH, Pz); 56.46 (CH_2); 43.45 ($C(CH_3)_3$); 26.19 ($C(CH_3)_3$) (Fig. S7). GC-MS Retention time 8.250 min, m/z (EI): 302, 283, 264, 245, 217, 170, 147, 121, 85, 69, 57, 43, 41, 29 (Fig. S8).

Yield of **8b** 5.7 g (60%), white crystals, mp 87 °C. IR spectrum, ν, cm^{-1}: 3171 (CH), 2982, 2963 (CH_2), 1701 (C=O), 1601 (C=N), 1234 (C–F), 1122 (C–F) (Fig. S9). ^1H NMR spectrum ($CDCl_3$), δ, ppm (*J*, Hz): 7.91 (2H, d, *J* = 7.5, Ph); 7.62 (2H, t, *J* = 7.3, Ph); 7.48 (1H, t, *J* = 7.6, Ph); 6.96 (1H, s, Pz); 5.77 (2H, s, CH_2) (Fig. S10). ^{13}C NMR spectrum ($CDCl_3$), δ, ppm (*J*, Hz): 189.91 (C=O); 142.63 (q, *J* = 39.3, C–CF_3, Pz); 134.72 (q, *J* = 40.4, C–CF_3, Pz); 134.71 (CH, Ph); 133.67 (C, Ph); 129.21 (2CH, Ph); 128.05 (2CH, Ph); 119.76 (qd, *J* = 269.1, *J* = 128.1, 2CF_3); 106.70 (CH, Pz); 57.97 (CH_2) (Fig. S11). GC-MS Retention time 16.667 min, m/z (EI): 303, 255, 217, 278, 147, 105, 85, 77, 69, 52, 39 (Fig. S12).

Yield of **8c** 5.6 g (56%), light beige crystals, mp 111 °C. IR spectrum, ν, cm^{-1}: 3156 (CH), 2983, 2965 (CH_2), 1703 (C=O), 1601 (C=N), 1235 (C–F), 1123 (C–F). ^1H NMR spectrum ($CDCl_3$), δ, ppm (*J*, Hz): 8.02–7.91 (2H, m, Ar); 7.18–7.09 (2H, m, Ar); 6.93 (1H, s, Pz); 5.55 (2H, s, CH_2). ^{13}C NMR spectrum ($CDCl_3$), δ, ppm (*J*, Hz): 191.15 (C=O); 167.65 (C–F); 165.04 (C, Ar); 141.62 (q, *J* = 39.3, C–CF_3, Pz); 132.15 (q, *J* = 40.4, C–CF_3, Pz); 131.05 (CH, Ar); 130.96 (CH, Ar); 119.76 (qd, *J* = 270.1, *J* = 129.1, 2CF_3); 116.41 (CH, Ar); 106.67 (CH, Pz); 57.77 (CH_2).

General Synthetic Procedure for 1,2-N-Dialkyl-Substituted Pyrazolium Bromides 5a–h, 6a–d.

Synthesis of 1,2-bis(3,3-dimethyl-2-oxobutyl)-1*H*-pyrazol-1-ium bromide (5a) [15]. A solution of 1-pinacolylpyrazole **3a** (1.43 g, 9 mmol) and bromopinacolone **2a** (1.60 g, 9 mmol) in dry acetone (50 mL) was stirred in a sealed 100 mL round-bottom flask at room temperature for 2 days. If no precipitation occurred, the mixture was refluxed for 3–5 hours before being cooled to room temperature. The reaction mixture was then refrigerated until crystallization was complete. The resulting viscous mass was triturated with acetone, and the precipitated fine white solid of compound **5a** was collected by filtration, washed with hot acetone, and air-dried.

Yield of **5a** 2.5 g (82%), fine white precipitate, mp 190 °C. IR spectrum, ν, cm^{-1}: 3074 (CH), 2970 (CH_3), 1724 (C=O), 1612 (C=N) (Fig. S13). ^1H NMR spectrum (D_2O), δ, ppm (*J*, Hz): 8.20 (1H, d, *J* = 2.9, Pz); 8.01 (1H, d, *J* = 3.0, Pz); 6.85 (1H, t, *J* = 2.9, Pz); 4.99 (2H, d, *J* = 12.8, CH_2); 4.71 (2H, d, *J* = 12.8, CH_2); 1.18 (9H, s, t-Bu); 0.87 (9H, s, t-Bu) (Fig. S14). ^{13}C NMR spectrum (D_2O), δ, ppm: 211.84 (C=O); 131.51 (CH, Pz); 130.17 (CH, Pz); 112.08 (CH, Pz); 44.63 (CH_2); 37.73 (C, t-Bu); 24.28 (t-Bu); 22.71 (t-Bu) (Fig. S15).

The synthesis of 1,2-bis(2-phenyl-2-oxoethyl)-1H-pyrazol-1-ium bromide (5b) [15], **1,2-bis(2-(4-fluorophenyl)-2-oxoethyl)-1H-pyrazol-1-ium bromide (5c), 1,2-bis(2-(4-nitrophenyl)-2-oxoethyl)-1H-pyrazol-1-ium bromide (5d), 1-(3,3-dimethyl-2-oxobutyl)-2-(2-(4-(trifluoromethoxy)phenyl)-2-oxoethyl)-1H-pyrazol-1-ium bromide (5e), 1-(3,3-dimethyl-2-oxobutyl)-2-(2-(4-fluorophenyl)-2-oxoethyl)-1H-pyrazol-1-ium bromide (5f), 1-(2-(4-fluorophenyl)-2-oxoethyl)-2-(2-phenyl-2-oxoethyl)-1H-pyrazol-1-ium bromide (5g) and 1-(2-(4-bromophenyl)-2-oxoethyl)-2-(2-phenyl-2-oxoethyl)-1H-pyrazol-1-ium bromide (5h)** was carried out according to the procedure for the preparation of **5a**, using the appropriate reagents.

Yield of **5b** 1.9 g (63%), fine white precipitate, mp 185 °C (dec.). IR spectrum, ν, cm^{-1}: 3078 (CH), 1693 (C=O), 1597 (C=N) (Fig. S16). ^1H NMR spectrum (DMSO-d_6), δ, ppm (*J*, Hz): 8.76 (1H, d, *J* = 3.2, Pz); 8.50 (1H, d, *J* = 3.1, Pz); 7.60–7.58 (4H, m, Ph); 7.51 (2H, t, *J* = 7.6, Ph); 7.22–7.19 (4H, m, Ph); 6.75 (1H, s, Pz); 5.18 (2H, d, *J* = 12.7, CH_2); 4.90 (2H, d, *J* = 12.8, CH_2) (Fig. S17). ^{13}C NMR spectrum (D_2O), δ, ppm: 191.12 (C=O); 134.87 (CH, Pz); 134.17 (C, Ph); 133.42 (CH, Pz); 132.56 (C, Ph); 129.47 (CH, Ph); 129.05 (CH, Ph); 128.73 (CH, Ph); 128.57 (CH, Ph); 112.53 (CH, Pz); 75.70 (CH_2) (Fig. S18).

Yield of **5c** 3.1 g (81%), fine white precipitate, mp 158 °C. IR spectrum, ν, cm^{-1}: 3078 (CH), 2966 (CH_2), 1716 (C=O), 1593 (C=N), 1269 (C–F) (Fig. S19). ^1H NMR spectrum (D_2O), δ, ppm (*J*, Hz): 8.28 (1H, s, Pz); 8.14 (1H, s, Pz); 7.38 (2H, s, Ar); 7.29–7.22 (2H, m, Ar); 6.91 (1H, s, Pz); 6.88–6.83 (4H, m, Ar); 4.64 (4H, s, CH_2) (Fig. S20, S21). ^{13}C NMR spectrum (D_2O), δ, ppm (*J*, Hz): 190.61 (C=O); 165.59 (d, *J* = 295.7, C–F, Ar); 162.53 (d, *J* = 246.5, C–F, Ar); 134.05 (CH, Pz); 132.84 (CH, Pz); 132.73 (C, Ar); 132.25 (C, Ar); 132.18 (d, *J* = 13.5, CH, Ar); 129.48 (d, *J* = 8.6, CH, Ar); 116.53 (d, *J* = 22.2, CH, Ar); 115.92 (d, *J* = 22.2, CH, Ar); 115.38 (CH, Pz); 59.01 (CH_2) (Fig. S22). ^{19}F NMR spectrum (D_2O), δ, ppm: –103.57 (C–F); –112.89 (C–F). (Fig. S23).

Yield of **5d** 1.1 g (25%), fine beige precipitate, mp 200 °C (dec.). IR spectrum, ν, cm^{-1}: 2974, 2939 (CH_2), 1616 (C=O), 1473 (NO_2), 1431, 1392 (NO_2), 1165, 1033 (C–N) (Fig. S24). ^1H NMR spectrum (DMSO-d_6), δ, ppm (*J*, Hz): 7.74 (4H, d, *J* = 2.3, Ar); 7.59 (4H, d, *J* = 2.1, Ar); 7.48 (1H, d, *J* = 1.9, Pz); 7.35 (1H, d, *J* = 1.9, Pz); 6.32–6.16 (1H, m, Pz); 5.91 (2H, m, CH_2); 5.80 (2H, d, *J* = 10.9, CH_2); 5.61 (2H, d, *J* = 10.9, CH_2) (Fig. S25).

Yield of **5e** 2.8 g (70%), fine white precipitate, mp 149 °C. IR spectrum, ν, cm^{-1}: 3074 (CH), 2963 (CH_2), 1716 (C=O), 1601 (C=N), 1269 (C–F), 1215, 1161 (C–O–C) (Fig. S26). ^1H NMR spectrum (D_2O), δ, ppm (*J*, Hz): 8.19 (1H, s, Pz); 8.04 (1H, s, Pz); 7.96 (2H, d, *J* = 8.9, Ar); 7.34 (2H, d, *J* = 8.4, Ar); 6.83 (1H, s, Pz); 0.82 (9H, s, $C(CH_3)_3$) (Fig. S27, S28).

Yield of **5f** 2.7 g (78%), fine white precipitate, mp 160 °C. IR spectrum, ν, cm^{-1}: 3090 (CH), 2963 (CH_3), 1732 (C=O), 1709 (C=O), 1593 (C=N), 1230 (C–F) (Fig. S29). ^1H NMR spectrum (D_2O), δ, ppm (*J*, Hz): 8.20 (1H, d, *J* = 3.0, Pz); 8.04 (1H, d, *J* = 3.1, Pz); 7.96 (2H, t, *J* = 7.0, Ar); 7.19 (2H, t, *J* = 8.7, Ar); 6.84 (1H, t, *J* = 1.6, Pz); 4.67 (2H, s, CH_2); 4.64 (2H, s, CH_2); 0.83 (9H, s, $C(CH_3)_3$) (Fig. S30, S31). ^{13}C NMR spectrum (DMSO-d_6), δ, ppm: 206.85 (C=O); 193.88 (C=O); 165.84 (d, *J* = 252.6, C–F); 132.91 (C, Ar); 132.78 (CH, Pz); 132.43 (CH, Pz); 131.76 (d, *J* = 2.8, CH, Ar); 116.57 (d, *J* = 22.2, CH, Ar); 112.44 (CH, Pz); 58.01 (CH_2); 53.87 (CH_2); 39.27 (C); 24.08 ($C(CH_3)_3$) (Fig. S32, S33). ^{19}F NMR spectrum (D_2O), δ, ppm: –104.7 (C–F) (Fig. S34).

Yield of **5g** 2.6 g (73%), fine white precipitate, mp 178 °C. IR spectrum, ν, cm^{-1}: 3094 (CH), 2951 (CH_2), 1709 (C=O), 1601 (C=N), 1215 (C–F) (Fig. S35). ^1H NMR spectrum (D_2O), δ, ppm (*J*, Hz): 8.28 (1H, d, *J* = 3.3, Pz); 8.12 (1H, d, *J* = 3.3, Pz); 7.47–7.07 (6H, m, Ph, Ar); 6.90 (1H, t, *J* = 3.2, Pz); 6.81–6.77 (2H, m, Ph); 4.63 (4H, s, CH_2) (Fig. S36, S37). ^{13}C NMR spectrum (D_2O), δ, ppm: 197.88 (C=O); 165.04 (C–F); 134.93 (C, Ar); 132.31 (CH, Pz); 131.65 (CH, Pz); 130.57; 129.01; 128.77; 126.35 (Ph, Ar); 117.31 (2CH, Ar); 113.61 (CH, Pz); 58.73 (CH_2); 53.83 (CH_2) (Fig. S38).

Yield of **5h** 1.9 g (47%), fine beige precipitate, mp 195 °C (dec.). IR spectrum, ν, cm^{-1}: 3094 (CH), 2906 (CH_2), 1701 (C=O), 1593 (C=N), 999 (C–Br) (Fig. S39). ^1H NMR spectrum (DMSO-d_6), δ, ppm (*J*, Hz): 7.93–7.91 (1H, m, Ph); 7.55–7.51 (4H, m, Ph); 7.50 (2H, d, *J* = 3.6, Ar); 7.34 (1H, s, Pz); 7.23 (1H, s, Pz); 7.11 (2H, d, *J* = 3.0, Ar); 6.68 (1H, s, Pz); 5.10 (2H, d, *J* = 12.6, CH_2); 4.84 (2H, d, *J* = 12.7, CH_2) (Fig. S40). ^{13}C NMR spectrum (DMSO-d_6), δ, ppm: 187.3 (C=O); 166.2 (C–F); 140.9 (CH, Pz); 140.2 (CH, Pz); 133.4 (CH, Ar); 131.2 (C, Ar); 115.1 (CH, Ar); 111.8 (CH, Pz); 75.9 (CH_2).

The synthesis of 1,2-bis(3,3-dimethyl-2-oxobutyl)-3,5-dimethyl-1H-pyrazol-1-ium bromide (6a), 1,2-bis(2-phenyl-2-oxoethyl)-3,5-dimethyl-1H-pyrazol-1-ium bromide (6b), 1,2-bis(2-(4-bromophenyl)-2-oxoethyl)-3,5-dimethyl-1H-pyrazol-1-ium bromide (6c) and 2-(2-(4-bromophenyl)-2-oxoethyl)-1-(2-oxo-2-phenylethyl)-3,5-dimethyl-1H-pyrazol-1-ium bromide (6d) was carried out according to the procedure for the preparation of **5a**, using the appropriate reagents.

Yield of **6a** 2.1 g (62%), fine white precipitate, mp 160 °C. IR spectrum, ν, cm^{-1}: 3095 (CH), 2973 (CH_3), 1723 (C=O), 1615 (C=N). ^1H NMR spectrum (D_2O), δ, ppm (*J*, Hz): 6.52 (1H, s, Pz); 4.97 (2H, d, *J* = 12.7, CH_2); 4.70 (2H, d, *J* = 12.6, CH_2); 2.16 (6H, s, CH_3); 1.17 (9H, s, t-Bu); 0.86 (9H, s, t-Bu). ^{13}C NMR spectrum (D_2O), δ, ppm: 212.54 (C=O); 142.01 (C, Pz); 140.67 (C, Pz); 108.15 (CH, Pz); 45.13 (CH_2); 38.23 (CH_2); 25.78 (t-Bu); 23.71 (t-Bu).

Yield of **6b** 2.0 g (53%), fine white precipitate, mp 185 °C. IR spectrum, ν, cm^{-1}: 3001 (CH), 2916 (CH_3), 1701 (C=O), 1535 (C=N) (Fig. S41). ^1H NMR spectrum (D_2O), δ, ppm (*J*, Hz): 7.60–7.53 (2H, m, Ph); 7.47 (4H, dd, *J* = 4.3, *J* = 3.1, Ph); 7.23–7.18 (4H, m, Ph); 6.51 (1H, s, Pz); 4.89 (2H, d, *J* = 12.4, CH_2); 4.61 (2H, d, *J* = 12.4, CH_2); 2.16 (6H, s, CH_3) (Fig. S42). ^{13}C NMR spectrum (D_2O), δ, ppm: 191.40 (C=O); 144.31 (C, Pz); 144.11 (C, Pz); 137.11; 135.22; 134.04; 129.14; 128.99; 128.97; 128.72; 128.69 (Ph); 111.83 (CH, Pz); 59.69 (CH_2); 11.15 (CH_3); 10.39 (CH_3) (Fig. S43).

Yield of **6c** 2.5 g (48%), fine beige precipitate, mp 190 °C (dec.). IR spectrum, ν, cm^{-1}: 3121, 1585 (CH), 2912 (CH_3), 1716 (C=O), 1603 (C=N), 1003 (C–Br) (Fig. S44). ^1H NMR spectrum (D_2O), δ, ppm (*J*, Hz): 7.43–7.41 (4H, m, Ar); 7.20–7.17 (4H, m, Ar); 6.54 (1H, s, Pz); 4.86 (2H, d, *J* = 10.9, CH_2); 2.18 (6H, s, CH_3) (Fig. S45). ^{13}C NMR spectrum (D_2O), δ, ppm: 193.89 (C=O); 150.93 (C, Pz); 146.83 (C, Pz); 133.51; 131.97; 125.49; 123.80 (Ar); 108.27 (CH, Pz); 56.38 (CH_2); 20.41 (CH_3) (Fig. S46).

Yield of **6d** 2.3 g (51%), fine beige precipitate, mp 201 °C (dec.). IR spectrum, ν, cm^{-1}: 3125 (CH), 2926 (CH_3), 1705 (C=O), 1601 (C=N), 1003 (C–Br) (Fig. S47). ^1H NMR spectrum (D_2O), δ, ppm (*J*, Hz): 7.62–7.11 (9H, m, Ph, Ar); 6.53 (1H, s, Pz); 4.74–4.67 (4H, m, CH_2); 2.09 (6H, s, CH_3) (Fig. S48). ^{13}C NMR spectrum (D_2O), δ, ppm: 191.27 (C=O); 147.06 (C, Pz); 144.59 (C, Pz); 135.21; 131.90; 131.84; 130.35; 129.14; 129.03; 128.90; 128.71; 127.14; 125.23; 122.93 (Ph, Ar); 111.90 (CH, Pz); 67.78 (CH_2); 30.17 (CH_3) (Fig. S49).

Determination of antimicrobial activity by the disk diffusion method. Test strains were preliminary cultured at (36 ± 1) °C for 24 h on slant meat-peptone agar. Standard bacterial suspensions were prepared from 24-h cultures: biomass was transferred with an inoculating loop into a tube containing sterile 0.9% sodium chloride solution, and the turbidity was adjusted to 0.5 McFarland standard [52, 53]. Test strain suspensions (100 μL) were inoculated onto the surface of nutrient media using an automatic pipette and evenly spread with a spreader. Petri dishes were kept at room temperature for 15–20 min to allow moisture absorption. Sterile paper disks pre-impregnated with the test samples were then placed onto the inoculated agar surface. Disks containing the antibiotic gentamicin (for bacteria) and the antifungal agent nystatin (for *Candida albicans*) were used as positive controls. The cultures were incubated at (36 ± 1) °C for 24 h for bacterial test strains and at (26 ± 1) °C for 24–48 h for *Candida albicans*. Results were recorded by measuring the diameters of inhibition zones around the disks (in millimeters). The progress of the study is shown on the Figures S50–S53.

Determination of minimum inhibitory concentration (MIC) by the serial microdilution method. The minimum inhibitory concentration (MIC) of the test samples was determined by the serial broth microdilution method in 96-well round-bottom microplates [47, 50, 51]. Test samples were added into the plate wells containing meat-peptone broth to achieve final concentrations of 1.0, 0.5, 0.25,

0.125, and 0.06 mg/mL. Then, 100 μL of a standardized suspension of 24-h test microorganism cultures (initial turbidity of 0.5 McFarland standard [52]) was added to each well. The cultures were incubated at (36 ± 1) °C for 24 h (for bacterial strains) and at (26 ± 1) °C (for *Candida albicans*). Sterile broth without inoculum was used as a negative control, while broth with inoculum but without test samples served as a positive control. The results were evaluated visually under transmitted light. The MIC was defined as the lowest concentration of the test sample that resulted in complete inhibition of visible microbial growth (the broth remained clear). The progress of the study is shown on the Figure S54.

Conclusion

In summary, an efficient two-stage synthetic approach to a novel series of symmetric (**5a–d**, **6a–c**) and unsymmetrical (**5e–h**, **6d**) 1,2-dialkylpyrazolium salts was successfully developed via sequential N-alkylation of pyrazoles 1**a, b**.

Investigation of the reaction scope demonstrated that the quaternization stage is critically governed by both electronic and steric effects of substituents at positions 3 and 5 of the pyrazole core, where electron-donating methyl groups (**1b**) facilitate quaternization by enhancing the nucleophilicity of the N-2 pyridine-type nitrogen atom. Sterically bulky phenyl rings (**1c**) and strongly electron-withdrawing trifluoromethyl groups (**1d**) arrest the reaction at the mono-alkylation step (**7a–b**, **8a–b**) due to steric hindrance and severe deactivation of the pyrazole core.

Spectral characterization (^{1}H and ^{13}C NMR) confirmed the electronic isolation of the pyrazole ring from the acyl moiety via the aliphatic -CH_2- linker, showing that the chemical shifts of the C-4 center depend exclusively on the electronic nature of the R substituents at positions 3 and 5.

Evaluation of the antibacterial and antifungal properties revealed that the synthesized pyrazolium salts possess a selective antibacterial spectrum, being completely inactive against *Candida albicans*. The highest susceptibility was observed for the Gram-positive strain *Bacillus subtilis* ATCC 6633. Notably, compound **6c** exhibited potent antibacterial activity against *B. subtilis*, comparable to the reference drug gentamicin (inhibition zone 20±1.5 mm vs. 20±0.58 mm), with a minimum inhibitory concentration (MIC) of 0.12 mg/mL.

These results strongly correlate with the preliminary cytotoxicity screening LC_{50} on *Artemia salina* [36] of mono-derivatives, which demonstrated that introducing specific electron-donating and electron-withdrawing groups enables directional modulation of membrane-active properties. The logical transition to pyrazolium salts **5a–h** and **6b–d** combining lipophilic halogenated phenyl radicals and electron-donating methyl groups allowed for minimizing non-specific toxicity while achieving targeted, high antibacterial potency. Consequently, compounds **6c** and **6d** represent promising lead structures for the further design and optimization of novel selective antibacterial agents.

Furthermore, these results expand the synthetic utility of pyrazole-based heterocycles, which continue to demonstrate versatile pharmacological importance as scaffold architectures in target-driven drug design, including therapeutic applications ranging from membrane-active antimicrobial leads and anticancer evaluations [54] to potent α-glucosidase inhibitors [55, 56].

Supporting Information

Supplementary information file, which includes the NMR, IR, and mass spectra for compounds with *in vitro* antimicrobial and antifungal activity data, are available at the journal website http://link.springer.com/ journal/

Conflict of Interests

The authors declare no conflict of interest.

Funding

The work was carried out within the framework of grant funding of the Science Committee of the Ministry of Science and Higher Education of the Republic of Kazakhstan (project registration No. AP19677175) and within the framework of the State Assignment of the Ministry of Science and Higher Education of the Russian Federation for Lomonosov Moscow State University (registration No. AAAA-A21-121012290046-4).

References

1. Schmidt A, Dreger A (2011) Recent advances in the chemistry of pyrazoles. Properties, biological activities, and syntheses. Curr Org Chem 15:1423–1463. https://doi.org/10.2174/138527211795378263
2. Schnürch M, Flasik R, Khan AF, Spina M, Mihovilovic MD, Stanetty P (2006) Cross-Coupling Reactions on Azoles with Two and More Heteroatoms. Eur J Org Chem 2006:3283–3307. https://doi.org/10.1002/ejoc.200600089
3. Kost AN, Grandberg II (1966) Progress in pyrazole chemistry. Adv Heterocycl Chem 6:347–429. https://doi.org/10.1016/S0065-2725(08)60579-6
4. Filyakova VI, Boltacheva NS, Slepukhin PA, Charushin VN (2023) Efficient one-pot synthesis of 3-(polyfluoroalkyl)pyrazol-4-amines. Chem Heterocycl Comp 59:546–553. https://doi.org/10.1007/s10593-023-03232-9
5. Lei J, Ding Y, Tang DY, Li H, Xu Z, Chen Z (2023) Efficient synthesis of pyrazoles by pH dependent isomerization of enaminodiones. Asian J Org Chem 12:e202200448. https://doi.org/10.1002/ajoc.202200448
6. Karrouchi K, Radi S, Ramli Y, Taoufik J, Al-Aizari FA, Mabkhot YN (2018) Synthesis and pharmacological activities of pyrazole derivatives: a review. Molecules 23:134. https://doi.org/10.3390/molecules23010134
7. Khandekar AA, Jadhav VB, Hajare SS (2026) Pyrazole derivatives as multi-target therapeutic agents: a comprehensive review of synthesis, structure-activity relationships, and pharmacological applications. Int J Sci R Tech 3:432–452. https://doi.org/10.5281/zenodo.20566881
8. Ansari A, Ali M, Asif M, Shamsuzzaman (2017) Review: biologically active pyrazole derivatives. New J Chem 41:16–41. https://doi.org/10.1039/c6nj03181a

9. Filali I (2026) Synthesis and biological activities of pyrazoline derivatives: a comprehensive review. J Heterocycl Chem 63:247–275. https://doi.org/10.1002/jhet.70120

10. Anjali, Yadav R, Singh H, Kaur R (2026) Recent advances in pyrazoline-based derivatives: synthetic approaches, pharmacological potential and molecular docking perspectives. Int J Drug Deliv Technol 16:534–561. https://doi.org/10.25258/ijddt.16.2.59

11. Odeh DM, Odeh MM, Hafez TS, Hassan AS (2025) Bioactive fused pyrazoles inspired by the adaptability of 5-aminopyrazole derivatives: recent review. Molecules 30:366. https://doi.org/10.3390/molecules30020366

12. Lei J, Ding Y, Tang DY, Li H, Xu Z, Chen Z (2023) Efficient synthesis of pyrazoles by pH dependent isomerization of enaminodiones. Asian J Org Chem 12:e202200448. https://doi.org/10.1002/ajoc.202200448

13. Castillo JC, Portilla J (2019) Recent advances in the synthesis of new pyrazole derivatives. *Targeted Heterocycl Syst* 22:194–223. https://doi.org/10.17374/targets.2019.22.194

14. Solomons TW, Calderazzo J, Fowler FW (1965) The diazapentalene system. 1-benzoyl-2-phenylpyrazolo[1,2-a]pyrazole derivatives. *J Am Chem Soc* 87(3):528–531. https://doi.org/10.1021/ja01081a023

15. Alzhapparova NA, Panshina SY, Ibrayev MK, Babaev EV (2025) Features on the way to the synthesis of 1-benzoyl-2-phenyl-3a, 6a-diazapentalene and 1-pivaloyl-2-tert-butyl-3a,6a-diazapentalene. *Eurasian J Chem* 30:14–22. https://doi.org/10.31489/2959-0663/4-25-17

16. Babaev EV, Panshina SYu, Alzhapparova NA, Ibraev MK, Usenova MS (2025) 3a,6a-Diazapentalenes (pyrazolo[1,2-a]pyrazoles). *Russ Chem Bull* 74:1958–1975. https://doi.org/10.1007/s11172-025-4681-8

17. Sokolov SD (1979) Advances in the chemistry of 1,2-azoles. *Russ Chem Rev* 48:289–305. https://doi.org/10.1070/rc1979v048n03abeh002323

18. Zięba S, Piotrowska A, Mizera A, Ławniczak P, Markiewicz KH, Gzella A, Dubis AT, Łapiński A (2021) Spectroscopic and structural study of a new conducting pyrazolium salt. *Molecules* 26:4657. https://doi.org/10.3390/molecules26154657

19. Yamuna TS, Kaur M, Anderson BJ, Jasinski JP, Yathirajan HS (2014) 5-Amino-1H-pyrazol-2-ium hydrogen succinate. *Acta Crystallogr Sect E Struct Rep Online* 70:o221–o222. https://doi.org/10.1107/S1600536814001615

20. van Terwingen S, Brüx D, Wang R, Englert U (2021) Hydrogen-bonded and halogen-bonded: orthogonal interactions for the chloride anion of a pyrazolium salt. *Molecules* 26:3982. https://doi.org/10.3390/molecules26133982

21. Jo D, Hong SB (2018) Charge distribution and conformational stability effects of organic structure-directing agents on zeolite synthesis. *Chem Commun* 54:487–490. https://doi.org/10.1039/C7CC08818C

22. Omar N, El-Rabbat N (1974) Polarographic study of new antimicrobial pyrazolium salts I: 1,2,5-trimethyl-3-arylpyrazolium perchlorates. *J Pharm Sci* 63:937–939.

23. Zilberg S, Haas Y (2012) Role of Rydberg states in the photostability of heterocyclic dimers: the case of pyrazole dimer. *J Phys Chem A* 116:11111–11117. https://doi.org/10.1021/jp304325x

24. Özdemir MC, Özgün B (2014) Phenyl/alkyl-substituted-3,5-dimethylpyrazolium ionic liquids. *J Mol Liq* 200:380–384. https://doi.org/10.1016/j.molliq.2014.10.014

25. Özdemir MC, Özgün B, Aktan E (2019) 1-Aryl-3,5-dimethylpyrazolium based tunable protic ionic liquids (TPILs). *J Mol Struct* 1180:564–572. https://doi.org/10.1016/j.molstruc.2018.12.027

26. Chiappe C, Sanzone A, Mendola D, Castiglione F, Famulari A, Raos G, Mele A (2013) Pyrazolium- versus imidazolium-based ionic liquids: structure, dynamics and physicochemical properties. *J Phys Chem B* 117:668–676. https://doi.org/10.1021/jp3107793

27. Pastor MJ, Sanchez I, Campo JA, Schmidt R, Cano M (2018) New pyrazolium salts as a support for ionic liquid crystals and ionic conductors. *Materials* 11:548. https://doi.org/10.3390/ma11040548

28. Adams CJ, Kurawa MA, Orpen AG (2010) Coordination chemistry in the solid state: synthesis and interconversion of pyrazolium salts, pyrazole complexes, and pyrazolate MOFs. *Dalton Trans* 39(30):6974–6984. https://doi.org/10.1039/c0dt00195c

29. Moser P, Stingelin W (1973) Cationic pyrazole azo compounds. German Patent Application 3,544,574A1.

30. Guadrado P, Gonzalez-Nogal AM (1998) Reactions of pyrazolium salts with silyllithium reagents. Regioselective synthesis of 5-silylated 3-pyrazolines. *Tetrahedron Lett* 39:1449–1452. https://doi.org/10.1016/S0040-4039(97)10825-5

31. Foces-Foces C, Infantes L, Claramunt RM, López C, Jagerovic N, Elguero J (1997) Solid-state structure of NH-pyrazolium hydrochlorides and hydrobromides by X-ray crystallography and 13C CPMAS NMR. *J Mol Struct* 415:81–92. https://doi.org/10.1016/S0022-2860(97)00099-9

32. Fernández-Castaño C, Foces-Foces C, Jagerovic N, Elguero J (1995) The X-ray crystal and molecular structure of 3,5-di-tert-butylpyrazole hydrochloride at 200 K. *J Mol Struct* 355:265–271. https://doi.org/10.1016/0022-2860(95)08915-I

33. Rusew R, Kurteva V, Shivachev B (2020) Novel quaternary ammonium derivatives of 4-pyrrolidino pyridine: synthesis, structural, thermal, and antibacterial studies. *Crystals* 10:339. https://doi.org/10.3390/cryst10050339

34. Xue Y, Xiao H, Zhang Y (2015) Antimicrobial polymeric materials with quaternary ammonium and phosphonium salts. *Int J Mol Sci* 16(2):3626–3655. https://doi.org/10.3390/ijms16023626

35. Jennings MC, Minbiole KPC, Wuest WM (2015) Quaternary ammonium compounds: an antimicrobial mainstay and platform for innovation to address

bacterial resistance. *ACS Infect Dis* 1(7):288–303. https://doi.org/10.1021/acsinfecdis.5b00047

36. Alzhapparova NA, Panshina SY, Ibrayev MK, Babaev EV, Shybanov DE (2026) Molecular design and biological efficacy: Synthesis of N-(β-oxoethyl)pyrazole derivatives and analysis of their structure-cytotoxicity relationship. *J Indian Chem Soc* 103:102474. https://doi.org/10.1016/j.jics.2026.102474
37. Gomha SM, Hassaneen HME (2011) Synthesis and antimicrobial activity of some new pyrazoles, fused pyrazolo[3,4-d]-pyrimidine and 1,2-dihydroimidazo-[2,1-c][1,2,4]triazin-6-one derivatives. *Molecules* 16:6549–6560. https://doi.org/10.3390/molecules16086549
38. Abdel-Hafez ESMN, Abuo-Rahma GEDAA, Abdel-Aziz M, Radwan MF, Farag HH (2009) Design, synthesis and biological investigation of certain pyrazole-3-carboxylic acid derivatives as novel carriers for nitric oxide. *Bioorg Med Chem* 17:3829–3837. https://doi.org/10.1016/j.bmc.2009.04.037
39. Castagnolo D, Manetti F, Radi M, Bechi B, Pagano M, De Logu A, Meleddu R, Saddi M, Botta M (2009) Synthesis biological evaluation and SAR study of novel pyrazole analogues as inhibitors of Mycobacterium tuberculosis: Part 2. Synthesis of rigid pyrazolones. *Bioorg Med Chem* 17:5716–5721. https://doi.org/10.1016/j.bmc.2009.05.058
40. Bekhit AA, Ashour HMA, Guemei AA (2005) Novel pyrazole derivatives as potential promising anti-inflammatory antimicrobial agents. *Arch Pharm (Weinheim)* 338:167–174. https://doi.org/10.1002/ardp.200400940
41. Sharshira EM, Hamada NMM (2012) Synthesis and antimicrobial evaluation of some pyrazole derivatives. *Molecules* 17:4962–4971. https://doi.org/10.3390/molecules17054962
42. Filyakova VI, Boltacheva NS, Slepukhin PA, Charushin VN (2023) Efficient one-pot synthesis of 3-(polyfluoroalkyl)pyrazol-4-amines. *Chem Heterocycl Comp* 59:546–553. https://doi.org/10.1007/s10593-023-03232-9
43. Ouyang GP, Cai XJ, Chen Z, Song BA, Bhadury PS, Yang SY, Jin LH, Xue W, Hu DY, Zeng S (2008) Synthesis and antiviral activities of pyrazole derivatives containing an oxime moiety. *J Agric Food Chem* 56:10160–10167. https://doi.org/10.1021/jf802489e
44. Millis DL, Weigel JP, Moyers T, Buonomo FC (2002) Effect of deracoxib, a new COX-2 inhibitor, on the prevention of lameness induced by chemical synovitis in dogs. *Vet Ther* 3:453–464. https://pubmed.ncbi.nlm.nih.gov/12584683/
45. Amri IA, Isnaeni PD, Sabri J (2024) In vitro evaluation of the antimicrobial efficacy of *Eupatorium odoratum* ethanol extract against Gram-positive and Gram-negative bacterial strains. *Open Vet J* 14:3100–3107. https://doi.org/10.5455/OVJ.2024.v14.i11.39
46. Clinical and Laboratory Standards Institute (2018) Performance Standards for Antimicrobial Disk Susceptibility Tests (CLSI Standard M02, 13th ed.). Clinical and Laboratory Standards Institute, Wayne, PA.
47. Clinical and Laboratory Standards Institute (2018) Methods for Dilution Antimicrobial Susceptibility Tests for Bacteria That Grow Aerobically (CLSI Standard M07, 11th ed.). Clinical and Laboratory Standards Institute, Wayne, PA.
48. Hossain TJ (2024) Methods for screening and evaluation of antimicrobial activity: A review of protocols, advantages, and limitations. *Eur J Microbiol Immunol (Bp)* 14:97–115. https://doi.org/10.1556/1886.2024.00035
49. Zhang X, Hou X, Ma L, Shi Y, Zhang D, Qu K (2023) Analytical methods for assessing antimicrobial activity of nanomaterials in complex media: advances, challenges, and perspectives. *J Nanobiotechnol* 21:97. https://doi.org/10.1186/s12951-023-01851-0
50. Barnes VL, Heithoff DM, Mahan SP, House JK, Mahan MJ (2023) Antimicrobial susceptibility testing to evaluate minimum inhibitory concentration values of clinically relevant antibiotics. *STAR Protocols* 4:102512. https://doi.org/10.1016/j.xpro.2023.102512
51. Kadeřábková N, Mahmood AJS, Mavridou DAI (2024) Antibiotic susceptibility testing using minimum inhibitory concentration (MIC) assays. *NPJ Antimicrob Resist* 2:37. https://doi.org/10.1038/s44259-024-00051-6
52. McFarland J (1907) The nephelometer: an instrument for estimating the number of bacteria in suspensions used for calculating the opsonic index and for vaccines. *J Am Med Assoc* 49:1176–1178. https://doi.org/10.1001/jama.1907.25320140022001f
53. European Committee on Antimicrobial Susceptibility Testing (2023) Breakpoint Tables for Interpretation of MICs and Zone Diameters. Version 13.0. https://www.eucast.org/clinical_breakpoints
54. Pavilek B, Bortňák D, Šofranko J, Šofranková L, Špaldová J, Elefantová K, Olejníková P, Žídeková I, Végh D, Dokupilová S, Mikuš P, Breier A, Milata V (2023) *Eur J Org Chem* 26:e202300410. https://doi.org/10.1002/ejoc.202300410
55. Deswal N, Takkar P, Kaur L, Verma P, Ojha H, Kumar R (2025) Design and synthesis of newer isatin-pyrano[2,3-c]pyrazolone hybrids as α-glucosidase inhibitors. *J Indian Chem Soc* 102:102017. https://doi.org/10.1016/j.jics.2025.102017
56. Bhukal A, Maity S, Kumar A, Asati V, Sindhu J, Lal K (2025) Synthesis of spirooxindole-pyrazoline clubbed 1,2,3-triazoles as α-glucosidase inhibitors: Experimental and computational studies. *J Indian Chem Soc* 102:102215. https://doi.org/10.1016/j.jics.2025.102215

Supplementary Files

This is a list of supplementary files associated with this preprint. Click to download.

- SupportingInformation.pdf